Monthly Notices
of the
ROYAL ASTRONOMICAL SOCIETY

MNRAS **453,** 3785–3797 (2015) doi:10.1093/mnras/stv1834

Gravity or turbulence? – III. Evidence of pure thermal Jeans fragmentation at ∼0.1 pc scale

Aina Palau,[1]★ Javier Ballesteros-Paredes,[1] Enrique Vázquez-Semadeni,[1] Álvaro Sánchez-Monge,[2] Robert Estalella,[3]† S. Michael Fall,[4] Luis A. Zapata,[1] Vianey Camacho,[1] Laura Gómez,[5,6] Raúl Naranjo-Romero,[1] Gemma Busquet[7] and Francesco Fontani[8]

[1]*Instituto de Radioastronomía y Astrofísica, Universidad Nacional Autónoma de México, PO Box 3-72, 58090 Morelia, Michoacán, Mexico*
[2]*I. Physikalisches Institut der Universität zu Köln, Zülpicher Strasse 77, D-50937 Köln, Germany*
[3]*Departament d'Astronomia i Meteorologia (IEEC-UB), Institut Ciències Cosmos, U. Barcelona, Martí i Franquès 1, E-08028 Barcelona, Spain*
[4]*Space Telescope Science Institute, 3700 San Martin Drive, Baltimore, MD 21218, USA*
[5]*CSIRO Astronomy and Space Science, PO Box 76, NSW 1710 Epping, Australia*
[6]*Departamento de Astronomía, Universidad de Chile, Camino El Observatorio 1515, Las Condes, Santiago, Chile*
[7]*Instituto de Astrofísica de Andalucía, CSIC, Glorieta de la Astronomía, s/n, E-18008 Granada, Spain*
[8]*INAF-Osservatorio Astrofisico di Arcetri, L.go E. Fermi 5, I-50125 Firenze, Italy*

Accepted 2015 August 6. Received 2015 July 18; in original form 2015 April 17

ABSTRACT

We combine previously published interferometric and single-dish data of relatively nearby massive dense cores that are actively forming stars to test whether their 'fragmentation level' is controlled by turbulent or thermal support. We find no clear correlation between the fragmentation level and velocity dispersion, nor between the observed number of fragments and the number of fragments expected when the gravitationally unstable mass is calculated including various prescriptions for 'turbulent support'. On the other hand, the best correlation is found for the case of pure thermal Jeans fragmentation, for which we infer a core formation efficiency around 13 per cent, consistent with previous works. We conclude that the dominant factor determining the fragmentation level of star-forming massive dense cores at 0.1 pc scale seems to be thermal Jeans fragmentation.

Key words: turbulence – stars: formation – ISM: lines and bands – ISM: structure – radio continuum: ISM.

1 INTRODUCTION

For more than 60 yr it has been thought that turbulence is an agent capable of providing support to molecular clouds against gravitational collapse (e.g. Chandrasekhar 1951; Bonazzola et al. 1987; Léorat, Passot & Pouquet 1990; McKee & Tan 2003), while simultaneously producing local density enhancements that may become Jeans unstable and collapse (e.g. Sasao 1973; Elmegreen 1993; Padoan 1995; Vázquez-Semadeni & Gazol 1995; Klessen, Heitsch & Mac Low 2000; Vázquez-Semadeni, Ballesteros-Paredes & Klessen 2003), and this is currently the most accepted scenario for the dynamical state of molecular clouds (e.g. Mac Low & Klessen 2004; Krumholz & McKee 2005; Hennebelle & Chabrier 2008, 2011; Hopkins 2012; Chabrier, Hennebelle & Charlot 2014; Federrath 2015; Guszejnov & Hopkins 2015; Salim, Federrath & Kewley 2015). However, some recent studies suggest that this may not be the case. For instance, molecular clouds seem to form by large-scale compressions in the diffuse, warm, H I medium. The compressed gas undergoes a transition to the cold, dense atomic phase (e.g. Hennebelle & Pérault 1999; Heitsch et al. 2005; Vázquez-Semadeni et al. 2006), which is highly prone to Jeans instability (Hartmann, Ballesteros-Paredes & Bergin 2001), and thus must begin soon to collapse, in spite of the turbulence generated inside it by the original compression (Koyama & Inutsuka 2002; Audit & Hennebelle 2005; Vázquez-Semadeni et al. 2007; Heitsch & Hartmann 2008). Moreover, once molecular clouds achieve column densities $\sim 10^{21}$ cm^{-2}, they are able to form molecular gas (Bergin et al. 2004) so that the formation of molecules may be essentially a byproduct of the gravitational collapse of the clouds (Hartmann et al. 2001). In this alternative scenario, the observed non-thermal motions of molecular clouds, rather than consisting of random, small-scale, isotropic motions that can act as a pressure,

★ E-mail: a.palau@crya.unam.mx
† The ICC (UB) is a CSIC-Associated Unit through the ICE (CSIC).

would actually be dominated by inwards motions *caused* by the gravitational collapse, which would occur both at large and small scales in a hierarchical and chaotic fashion (Vázquez-Semadeni et al. 2009; Ballesteros-Paredes et al. 2011a). This implies that the bulk of the observed non-thermal motions cannot provide support against the self-gravity of the clouds.

In previous papers of this series, we have presented evidence that the dynamics of molecular clouds are indeed dominated by gravity by showing that this scenario unifies molecular clouds and massive clumps in a single scaling relation (Heyer et al. 2009) that extends those by Larson (1981; Ballesteros-Paredes et al. 2011a), and by showing that numerical simulations of cloud evolution including self-gravity develop power-law high-density tails in their column density probability distribution functions as a consequence of the gravitational collapse (see also Klessen 2000; Kritsuk, Norman & Wagner 2011; Ballesteros-Paredes et al. 2011b; Federrath & Klessen 2013), in agreement with observations (e.g. Kainulainen et al. 2009; Schneider et al. 2013). In the present contribution, we present a further line of evidence, by examining the mechanism responsible for fragmentation of dense cores. Indeed, a still unsolved and highly debated question is what are the main drivers of fragmentation in massive dense cores,[1] which are believed to be the precursors of stellar clusters. The crucial parameter to estimate the fragmentation level of a dense core is the Jeans mass, which in its general form takes into account the different mechanisms of support against gravity, through the use of the 'effective sound speed', $c_{\rm eff}$ (e.g. Mac Low & Klessen 2004). Among the most debated forms of support are turbulent and thermal support. Thus, if the average turbulence level, average temperature and average density of a massive dense core are known, one can easily calculate the Jeans mass in both cases and estimate, given the mass of the core, the number of fragments expected in each case, so that one can assess which form of support against gravity is controlling the fragmentation process.

Up to now, this simple question could not be answered because of a lack of statistically significant samples of massive dense cores where the fragmentation level has been assessed in a uniform way and down to spatial resolutions comparable to separations between cluster members (∼1000 AU). Recently, Palau et al. (2013, 2014) compiled a sample of 19 massive dense cores with ongoing star formation and studied the fragmentation level within the cores down to ∼1000 au, and ∼0.5 $M_\odot$ of mass sensitivity. This would be a first approach to study the number of protostars (compact fragments will most likely become protostars; see Palau et al. 2013, 2014) within a massive dense core (assumed to become a cluster). In these works, the fragmentation level was assessed by counting the number of millimetre sources within a field of view of 0.1 pc of diameter,[2] $N_{\rm mm}$. Furthermore, by fitting the spectral energy distributions and submillimetre intensity profiles of the cores, Palau et al. (2014) modelled their density and temperature structure, so that densities and temperatures at different spatial scales could be estimated and thermal Jeans masses could be calculated. In this work, we compile observational data based on dense gas tracers for the sample of cores of Palau et al. (2013, 2014) and analyse them in a uniform way, in order to assess the turbulence level, estimate the turbulent-Jeans mass, and finally compare the fragmentation level observed to the fragmentation level expected for each form of support, turbulent or thermal.

The plan of the present contribution is as follows: Section 2 presents the compiled data we used. In Section 3, we present the fragmentation level of our cores, and how this fragmentation correlates (or not) with their physical parameters. Finally, in Section 4 we discuss the physical implications of our results and present our main conclusions.

2 THE SAMPLE AND DATA COMPILATION

The present work is based on the sample of massive dense cores presented in Palau et al. (2013, 2014), whose distances, luminosities and masses range from 0.45 to 3 kpc, from 300 to 10^5 $L_\odot$and from 80 to 1500 $M_\odot$, respectively (given in Table A1). The sample was selected from deeply embedded intermediate/high-mass star-forming regions published in the literature that have been studied in the millimetre range down to mass sensitivities of ∼0.5 $M_\odot$, and spatial resolutions of ∼1000 au. Palau et al. (2014) modelled the massive dense cores with temperature and density profiles decreasing with radius following power laws, and determined a number of properties of the density and temperature structure in a uniform way for all the sample.

In order to estimate the turbulence level in each core in a uniform way and compare it to the 'turbulent fragmentation' level, we used Very Large Array (VLA) NH_3(1,1) data in C/D configuration, available for 14 (out of 19) massive dense cores (Torrelles et al. 1989; Zhou et al. 1990; Mangum et al. 1992; Tieftrunk et al. 1998; Wiseman & Ho 1998; Gómez et al. 2003; Sánchez-Monge et al. 2013; see also Palau et al. 2014). VLA beams are typically $\lesssim$5 arcsec, and the minimum angular scales filtered out by the interferometer are $\gtrsim$35 arcsec (estimated following appendix in Palau et al. 2010, and using a minimum baseline of 35 m). The latter corresponds to ∼0.3 pc (for typical distances of the regions in the sample), slightly larger than the field of view of 0.1 pc that we are studying. Thus, with these VLA NH_3 data we are recovering most of the emission at the spatial scales we are studying, with an angular resolution good enough (∼5 arcsec) to resolve typical sizes of massive dense cores (e.g. Sánchez-Monge et al. 2013). The NH_3(1,1) hyperfine structure was fitted and hyperfine 'observed' FWHM line widths, $\Delta v_{\rm obs}$, were inferred for each core. We note that we took special care to make the sample as uniform as possible and we measured the NH_3(1,1) line width in all cases by using the 'nh3(1,1) method' in the CLASS package of the GILDAS software, on the spectrum resulting from averaging the NH_3(1,1) emission over the central region of ∼0.1 pc of diameter of the dense core where we study the fragmentation level. When literature did not provide an average spectrum over the massive dense core that we are studying, we downloaded and reduced the VLA data to extract the spectrum. This was done for HH80-81, W3IRS5, A2591, Cyg-N53, Cyg-N48 and DR21-OH (VLA projects AG0552, AT0180, AT0084, AW0240, AF386, respectively: standard calibration as described in Sánchez-Monge et al. 2013 was applied). In two sources (I22134 and DR21-OH), we fitted two velocity components. From these line widths, we calculated the observed velocity dispersions as $\sigma_{\rm 1D,obs} = \Delta v_{\rm obs}/(8\ln 2)^{1/2}$. The values of the compiled observed velocity dispersions from NH_3(1,1) VLA data are listed in Table 1, and the spectra with the corresponding fits to the hyperfine structure are shown in Appendix B.

[1] We will follow the nomenclature of Williams, Blitz & McKee (2000) and Bontemps et al. (2010) where a massive dense core refers to a dense gas structure of ∼0.1 pc in size and $\gtrsim$20 $M_\odot$ in mass, which does not necessarily collapse into one star but can fragment into compact condensations and form a small cluster of stars.

[2] The size of 0.1 pc was taken to be the smallest size where fragmentation could be studied (because of the limitations by the primary beam response) in the works of Palau et al. (2013, 2014).

Table 1. Modelled properties of the massive dense cores and compiled observational velocity dispersions.

Source	$N_{\rm mm}$	$M_{0.1\,{\rm pc}}{}^{a}$ ($M_\odot$)	$n_{0.1\,{\rm pc}}{}^{a}$ (10^5 cm^{-3})	$T_{0.1\,{\rm pc}}{}^{a}$ (K)	$\sigma^{\rm NH_3}_{\rm 1D,obs}{}^{b}$ (km s^{-1})	$\sigma^{\rm NH_3}_{\rm 1D,nth}{}^{b}$ (km s^{-1})	$\mathcal{M}_{\rm NH_3}{}^{b}$	$\sigma^{\rm N_2H^+}_{\rm 1D,obs}{}^{b}$ (km s^{-1})	$\sigma^{\rm N_2H^+}_{\rm 1D,nth}{}^{b}$ (km s^{-1})	$\mathcal{M}_{\rm N_2H^+}{}^{b}$
1-IC1396N	4	11	3.6	25	–	–	–	0.79	0.78	4.5
2-I22198[c]	1.5	11	3.6	26	0.47	0.45	2.6	0.59	0.59	3.4
3-N2071-1	4	17	5.7	24	0.44	0.43	2.5	–	–	–
4-N7129-2	1	11	3.6	35	–	–	–	0.59	0.58	2.8
5-CB3-mm	2	15	5.2	40	–	–	–	0.73	0.72	3.3
6-I22172N	3	9	3.2	48	0.59	0.58	2.4	0.87	0.86	3.6
7-OMC-1S	9	38	13	49	1.11	1.10	4.5	0.90	0.89	3.7
8-A5142	7	39	13	47	1.61	1.61	6.8	1.09	1.08	4.6
9-I05358NE	4	27	9.1	35	0.72	0.71	3.5	1.07	1.07	5.3
10-I20126	1	14	4.8	68	2.00	1.99	7.0	0.85	0.84	2.9
11-I22134	3.5	10	3.2	50	0.71	0.70	2.8	0.62	0.61	2.5
12-HH80-81	3	12	4.2	66	0.74	0.72	2.6	–	–	–
13-W3IRS5	3.5	12	4.0	138	0.87	0.84	2.1	1.18	1.17	2.9
14-A2591	1.5	16	5.2	147	0.68	0.62	1.5	–	–	–
15-Cyg-N53	6	30	10	27	0.17[d]	0.13[d]	0.7[d]	0.81	0.80	4.4
16-Cyg-N12	2.5	15	5.0	29	–	–	–	1.23	1.23	6.6
17-Cyg-N63	1	14	4.6	31	–	–	–	0.82	0.82	4.2
18-Cyg-N48	5	35	12	36	1.25	1.25	6.1	1.21	1.21	5.9
19-DR21-OH	11	69	23	49	1.51	1.51	6.3	–	–	–

Notes. [a]$M_{0.1\,{\rm pc}}$ is the mass inside a region of 0.1 pc of diameter computed according: $M_{0.1{\rm pc}} = M(R = 0.05{\rm pc}) = 4\pi\rho_0 r_0^p \frac{R^{3-p}}{3-p}$, where p, r_0 and ρ_0 are index of the density power law, the reference radius adopted to be 1000 AU and the density at the reference radius (given in table 1 of Palau et al. 2014); $n_{0.1\,{\rm pc}}$ and $T_{0.1\,{\rm pc}}$ correspond to average density and temperature inside a region of 0.1 pc of diameter. $T_{0.1\,{\rm pc}}$ is estimated as $T_{\rm R} = \frac{\int_0^R T(r)\rho(r)r^2{\rm d}r}{\int_0^R \rho(r)r^2{\rm d}r}$, where $T(r)$ and $\rho(r)$ were calculated as power laws of the form $T(r) = T_0(r/r_0)^{-q}$ and $\rho(r) = \rho_0(r/r_0)^{-p}$, with T_0 and ρ_0 being the values at the reference radius r_0 of 1000 AU. T_0, ρ_0, p and q are given in table 1 of Palau et al. (2014). The final expression is $T_{\rm R} = \frac{T_0(3-p)}{3-p-q}(\frac{r}{r_0})^{-q}$.

[b]$\sigma^{\rm NH_3}_{\rm 1D,obs}$ and $\sigma^{\rm N_2H^+}_{\rm 1D,obs}$ are calculated from the measured FWHM line width, $\Delta v_{\rm obs}$, as $\sigma_{\rm 1D,obs} = \Delta v_{\rm obs}/(8\ln 2)^{1/2}$. $\sigma_{\rm 1D,nth} = \sqrt{\sigma^2_{\rm 1D,obs} - \sigma^2_{\rm th}}$, with $\sigma_{\rm th} = \sqrt{k_{\rm B}T/(\mu\, m_{\rm H})}$ ($k_{\rm B}$ being the Boltzmann constant, μ the molecular weight (17 for NH_3, 29 for N_2H^+), $m_{\rm H}$ the mass of the hydrogen atom and T the temperature of the region, taken from column (5) of this table). The Mach number $\mathcal{M}$ is calculated as $\sigma_{\rm 3D,nth}/c_{\rm s}$, with $c_{\rm s}$ being the sound speed calculated as $c_{\rm s} = \sqrt{k_{\rm B}T/(\mu\, m_{\rm H})}$, using $\mu = 2.3$, and $\sigma_{\rm 3D,nth} = \sqrt{3}\,\sigma_{\rm 1D,nth}$.

[c]The parameters of the density and temperature structure for this source are different from Palau et al. (2014) because here we have used the original JCMT data of Jenness, Scott & Padman (1995) and we have not assumed any error beam in the modelling (see Appendix B).

[d]Marginal detection of the NH_3(1,1) line, not taken into account in the analysis of this work.

Refs: IC 1396N: Alonso-Albi et al. (2010); I22198: Sánchez-Monge et al. (2013), Fontani et al. (2011); NGC2071-1: Zhou et al. (1990); NGC7129-2: Fuente et al. (2005); CB3-mm: Alonso-Albi et al. (2010); I22172N: Sánchez-Monge et al. (2013); Fontani et al. (2006); OMC-1S: Wiseman & Ho (1998); Tatematsu et al. (2008); A5142: Sánchez-Monge et al. (2013); Fontani et al. (2011); I05358NE: Sánchez-Monge et al. (2013); Fontani et al. (2011); I20126: Sánchez-Monge et al. (2013); Fontani et al. (2006); I22134: Sánchez-Monge et al. (2013); Fontani et al. (2015); HH80-81: Gómez et al. (2003); W3IRS5: Tieftrunk, Gaume & Wilson (1998); Gerner et al. (2014); A2591: Torrelles et al. (1989); Cyg-N53: VLA archive; Bontemps et al. (2010); Cyg-N12: Bontemps et al. (2010); Cyg-N63: Bontemps et al. (2010); Cyg-N48: Mangum, Wootten & Mundy (1992), Bontemps et al. (2010); DR21-OH: Mangum et al. (1992).

Because in some cases the VLA NH_3(1,1) emission might be affected by the passage of an outflow (e.g. the NH_3(1,1) line width of IRAS 20126+4104 is larger along the direction of the outflow, see fig. B1 of Sánchez-Monge et al. 2013), we additionally compiled data from a different dense gas tracer, N_2H^+(1–0), observed using a single-dish telescope [Institut de Radioastronomie Millimétrique (IRAM) 30 m in all cases except for OMC-1S, for which Nobeyama 45m was used]. This is a reasonable approach to avoid contamination by outflow for several reasons. First, N_2H^+ is known to be destroyed by CO (e.g. Jørgensen 2004; Busquet et al. 2011). Second, the outflow is typically compact and thus its emission should be diluted in the single-dish beam. Thus, the N_2H^+ line widths should be less affected by the passage of the outflow and thus more reliable to measure the 'initial' non-thermal motions unaffected by stellar feedback. The N_2H^+(1–0) data were available for 15 out of 19 regions and were compiled from the literature (Fuente et al. 2005; Fontani et al. 2006, 2011, 2015; Tatematsu et al. 2008; Alonso-Albi et al. 2010; Bontemps et al. 2010; Gerner et al. 2014), and its hyperfine structure was fitted using the CLASS package of the GILDAS software. The IRAM 30 m Telescope provides a beam of ∼26 arcsec at the frequency of N_2H^+(1–0), comparable to the spatial scale at which the massive dense cores are being studied (0.1 pc, at the typical distances of the cores of our sample), and about a factor of 5 larger than the VLA beam. By using the same method outlined above for NH_3(1,1), we inferred the observed velocity dispersions for N_2H^+(1–0), listed in Table 1 and the spectra and fits are shown in Appendix B. The method used to fit the hyperfine structure for both N_2H^+ and NH_3 takes the opacity effects into account. The observed N_2H^+(1–0) velocity dispersions range from 0.6 to 1.2 km s^{-1}, a narrower range than that of the velocity dispersions inferred from VLA NH_3 data (ranging from 0.5 to 2.0 km s^{-1}), as expected (because of the outflow contamination of the NH_3 VLA data).

The main difference between the line widths reported in this work and the line widths reported in column (10) of table 2 of Palau et al. (2014[3]) is that we here re-reduced the interferometric data

[3] Line widths reported in column (9) of table 2 of Palau et al. (2014), or in column (10) of table 4 of Palau et al. (2013) correspond to quiescent cores in the surroundings of the massive dense cores where fragmentation

and re-did the fits of the spectra in all cases using the same method, instead of just taking the values reported in the literature, which use different methods. Thus, the present analysis is uniform in the sense that the method to infer the line widths is the same for all sources.

3 RESULTS AND ANALYSIS

3.1 Fragmentation level versus density and velocity dispersions

The compiled observed velocity dispersions of $NH_3(1,1)$ and $N_2H^+(1–0)$ together with the modelling of the temperature structure of the massive dense cores (Palau et al. 2014) allowed us to separate the thermal from the non-thermal contribution of the observed velocity dispersion. We estimated the thermal component of the velocity dispersion, $\sigma_{\rm th}$, from $\sqrt{k_{\rm B}\,T/(\mu\,m_{\rm H})}$, with $k_{\rm B}$ the Boltzmann constant, μ the molecular weight (17 for NH_3, 29 for N_2H^+), $m_{\rm H}$ the mass of the hydrogen atom and T the temperature of the region, which was adopted from the average density-weighted temperature inside a region of 0.1 pc of diameter (the same region where we assessed the fragmentation level). This average temperature is estimated from the density and temperature power laws modelled by Palau et al. (2014, see notes of Table 1 for further details) for each core. The non-thermal component was estimated by using $\sigma_{\rm 1D,nth} = \sqrt{\sigma^2_{\rm obs} - \sigma^2_{\rm th}}$. Then, the total (thermal + non-thermal) velocity dispersion is calculated by adding quadratically the thermal and non-thermal components, using for the thermal component a molecular weight of 2.3, which corresponds to the sound speed and thus: $\sigma_{\rm 1D,tot} = \sqrt{c_{\rm s}^2 + \sigma^2_{\rm nth}}$. The Mach number $\mathcal{M}$ is calculated as $\sigma_{\rm 3D,nth}/c_{\rm s}$, with $\sigma_{\rm 3D,nth} = \sqrt{3}\,\sigma_{\rm 1D,nth}$. The resulting Mach numbers range from ∼2 to 7.

In Fig. 1, we plot the number of millimetre sources within a field of view of 0.1 pc in diameter, $N_{\rm mm}$ (a proxy to the fragmentation level), as function of (a) the core density within a region of 0.1 pc of diameter (modelled in Palau et al. 2014) – upper panel, (b) the non-thermal velocity dispersion measured from $NH_3(1,1)$ (interferometric data) – middle panel and from $N_2H^+(1–0)$ (single-dish data) – lower panel. The figure shows that, while there is a correlation between $N_{\rm mm}$ and the density within 0.1 pc (correlation coefficient: 0.89), there is no clear trend between $N_{\rm mm}$ and the velocity dispersion measured with NH_3 (correlation coefficient: 0.27), nor with N_2H^+ (correlation coefficient: 0.35). This suggests that the velocity dispersion of the massive dense cores might not be a crucial ingredient in determining the fragmentation level.

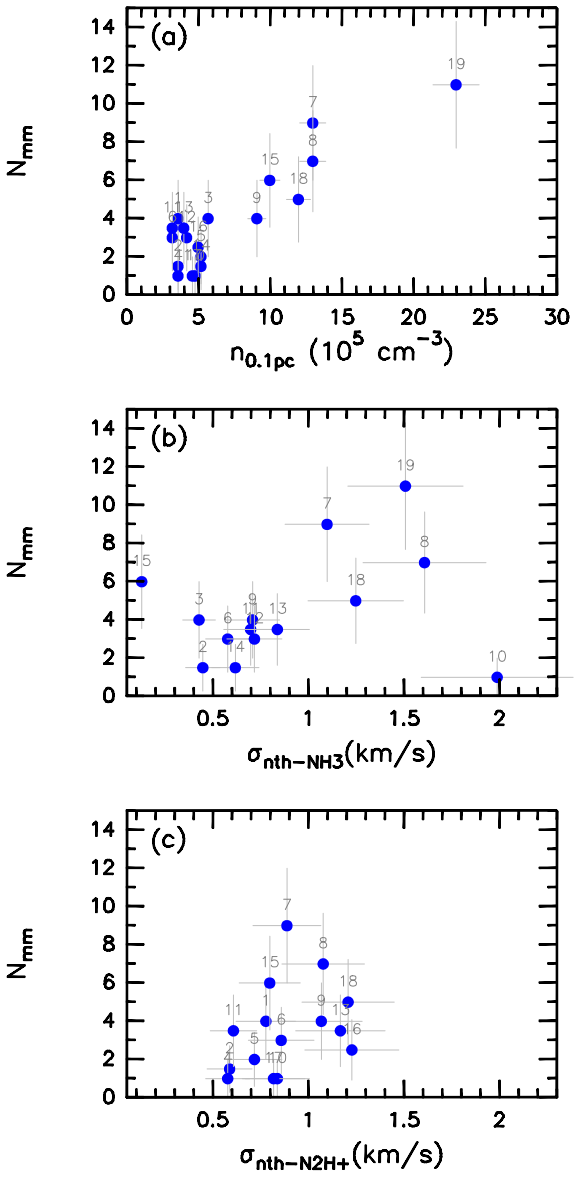

Figure 1. Observed 'fragmentation level' ($N_{\rm mm}$) versus different quantities (Table 1). (a) $N_{\rm mm}$ versus the density of the core within a region of 0.1 pc of diameter. (b) $N_{\rm mm}$ versus the non-thermal velocity dispersion as inferred from VLA $NH_3(1,1)$ data. (c) $N_{\rm mm}$ versus the non-thermal velocity dispersion as inferred from single-dish N_2H^+ (1–0) data.

3.2 Fragmentation level versus 'turbulent' Jeans number

To further compare the role of the physical properties of the cores (density, temperature, velocity dispersion) in determining the fragmentation, we estimated the expected number of fragments under different assumptions for the gravitationally unstable mass, to which, for convenience, we continue referring as a 'Jeans' mass in general. To estimate the Jeans mass, we started from the Jeans length, $L_{\rm Jeans} = \sqrt{\frac{\pi c^2_{\rm eff}}{G\rho_{\rm eff}}}$ (e.g. Kippenhahn, Weigert & Weiss 2012), and assumed spherical symmetry, $M_{\rm Jeans} = \frac{4\pi}{3}\rho_{\rm eff}(\frac{L_{\rm Jeans}}{2})^3$, where $c_{\rm eff}$ is the 'effective sound speed', $\rho_{\rm eff}$ is the 'effective density' and G is the gravitational constant. Therefore,

$$M_{\rm Jeans} = \frac{\pi^{5/2}}{6\,G^{3/2}}\,c^3_{\rm eff}\,\rho^{-1/2}_{\rm eff}. \quad (1)$$

First, we have searched for a correlation between the observed fragmentation level $N_{\rm mm}$ and the expected number of fragments in a turbulent support scenario (e.g. Mac Low & Klessen 2004). Thus, we have computed the expected mass of the fragments by assuming that the critical 'Jeans' mass is determined by non-thermal ('turbulent') support, where the 'effective sound speed' $c_{\rm eff}$ corresponds to the non-thermal component of the observed velocity dispersion $\sigma_{\rm 1D,nth}$. This, in practical units and using the number density of H_2

is being studied, and are not comparable to the line widths reported here, corresponding to the massive dense cores where active star formation is taking place and where fragmentation is being studied.

molecules (as calculated by the model in Palau et al. 2014, and using a molecular weight of 2.8), can be written as

$$\left[\frac{M^{\rm nth}_{\rm Jeans}}{\rm M_\odot}\right] = 0.8255 \left[\frac{\sigma_{\rm 1D,nth}}{0.188\,{\rm km\,s^{-1}}}\right]^3 \left[\frac{n_{\rm H_2}}{10^5\,{\rm cm^{-3}}}\right]^{-1/2}. \quad (2)$$

Then, the number of expected fragments, $N_{\rm Jeans}$, is estimated from the ratio of the mass of the core inside a region of 0.1 pc of diameter, $M_{\rm 0.1\,pc}$,[4] and the Jeans mass, $M_{\rm Jeans}$:

$$N_{\rm Jeans} = \frac{M_{\rm 0.1pc}}{M_{\rm Jeans}}. \quad (3)$$

The result is presented in Figs 2(a) and (d) (for NH_3(1,1) and N_2H^+ (1–0), respectively).

We also estimated the Jeans mass including both thermal and non-thermal support:

$$\left[\frac{M^{\rm tot}_{\rm Jeans}}{\rm M_\odot}\right] = 0.8255 \left[\frac{\sigma_{\rm 1D,tot}}{0.188\,{\rm km\,s^{-1}}}\right]^3 \left[\frac{n_{\rm H_2}}{10^5\,{\rm cm^{-3}}}\right]^{-1/2} \quad (4)$$

(Figs 2b and e), and including only non-thermal support but taking into account that large-scale supersonic flows compress the gas and generate density enhancements, which are the ones that proceed to collapse (Mac Low & Klessen 2004). In this case, the 'effective density' is obtained by multiplying the average density of the core by the square of the Mach number:

$$\left[\frac{M^{\rm conv.flows}_{\rm Jeans}}{\rm M_\odot}\right] = 0.8255 \left[\frac{\sigma_{\rm 1D,nth}}{0.188\,{\rm km\,s^{-1}}}\right]^3 \left[\frac{n_{\rm H_2}\,\mathcal{M}^2}{10^5\,{\rm cm^{-3}}}\right]^{-1/2}, \quad (5)$$

(Figs 2c and f).

Figs 2(a) (NH_3) and (d) (N_2H^+) reveal a very weak correlation of $N_{\rm mm}$ with $N_{\rm Jeans}$ (correlation coefficient of 0.24 and 0.23, respectively), and a slope $\ll 1$ (0.14 ± 0.18 for NH_3, and 0.22 ± 0.25 for N_2H^+, see Table 2). For the case of non-thermal+thermal support the situation is very similar (Figs 2b and e), and for the case of 'density enhanced by turbulence' (equation 5 and Figs 2c and f), the correlation coefficient increases up to 0.50 and the slope up to 0.34 ± 0.18 (Table 2), with respect to the case of turbulence providing only support (equations 2 and 4). This was expected, because when taking into account the density enhancements produced by turbulence the role of turbulence providing support becomes less important and the correlation slightly improves.

Therefore, we show that considering the non-thermal motions as a form of support does not provide a good correlation between the expected number of fragments and the observed number in any of the cases considered. More importantly, we note that the turbulent-Jeans number for the majority of the cores is less than or similar to unity in all three cases, which would imply that, if turbulent support were active, these cores should not fragment at all, contrary to what is observed. As we will see in the next section, this would imply a core formation efficiency (CFE, see below) $\gtrsim$100 per cent, which is meaningless.

3.3 Fragmentation level versus thermal Jeans number

Given the poor correlations found between the observed number of fragments and the expected number of fragments in case of turbulent support, we considered only thermal support (no contribution from 'turbulence'). In this case, the 'effective sound speed' $c_{\rm eff}$ simply corresponds to the sound speed of the gas, which can be written in terms of the kinetic temperature, and the Jeans mass is finally written as

$$\left[\frac{M^{\rm th}_{\rm Jeans}}{\rm M_\odot}\right] = 0.6285 \left[\frac{T}{10\,{\rm K}}\right]^{3/2} \left[\frac{n_{\rm H_2}}{10^5\,{\rm cm^{-3}}}\right]^{-1/2}. \quad (6)$$

This was done using two different assumptions for the temperature. First, we used a fixed temperature of ~20 K, as a first approximation to the 'initial' (i.e. before being heated by the protostellar feedback) temperature of the dense core (e.g. Sánchez-Monge et al. 2013). Second, we used the average temperature estimated for each core within a region of 0.1 pc of diameter, $T_{\rm 0.1\,pc}$ (ranging from 25 to 150 K, Table 1). This assumption should give an upper limit to the temperature at the time when fragmentation took place.[5]

The results are plotted in Figs 2(g) and (h). Fig. 2(g) shows a correlation of $N_{\rm mm}$ and $N_{\rm Jeans}$, with a slope of 0.60 ± 0.14, clearly larger and closer to 1 than the slope obtained for the turbulence-supported case (0.2–0.3, Table 2). In this panel, the temperature is fixed for all the cores and equal to 20 K. The data are clearly offset with respect to the one-to-one relation (dotted black line), which can be explained if only a percentage of the total mass of the core is converted into compact fragments. We define the CFE as the fraction of mass of a dense core found in (pre-stellar and protostellar) compact fragments (as in Bontemps et al. 2010), and in this case:

$$N_{\rm Jeans} = \frac{M_{\rm 0.1pc}\,{\rm CFE}}{M_{\rm Jeans}}. \quad (7)$$

Thus, we fitted a line with slope 1 (dashed red line in Fig. 2) and the offset should be a first approximation to the CFE. By doing this for the data set of Fig. 2(g), we found a CFE of 13 per cent, with a correlation coefficient of 0.72. This value for the CFE is fully consistent with the independent direct measurements of the CFE by Bontemps et al. (2010) and Palau et al. (2013), who estimated this quantity by dividing the total mass in compact fragments (detected with an interferometer in an extended configuration) by the mass of the core (measured with a single dish). Our inferred CFE is also similar to those found by Louvet et al. (2014) in the W43-MM1 region.

We additionally estimated $N_{\rm Jeans}$ using the different average temperatures inferred for each core (Table 1), and the result is shown in Fig. 2(h). In this approach, $N_{\rm Jeans}$ is smaller (compared to the previous case of fixed temperature equal to 20 K), because the Jeans masses are larger due to the higher adopted temperatures, and hence the inferred CFE is larger as well. The effect of using these higher temperatures is to predict too small a number of fragments (too small $N_{\rm Jeans}$), especially for the two extreme cases (cores 13 and 14) which are also the most luminous regions. In this case, we obtained a correlation coefficient of 0.57, and a CFE of 41 per cent.

[4] The mass inside a region of 0.1 pc of diameter is typically ~10 per cent of the total mass of the core (given in table 4 of Palau et al. 2013) and is only marginally correlated to the mass of the core, in part because far from the central part of the core, the core departs from sphericity, a basic assumption of the core modelling of Palau et al. (2014).

[5] The stellar feedback should affect the density structure on larger time-scales compared to the time-scale when stellar feedback modifies the temperature because the first should change through mechanical processes while the latter changes through radiative processes. In addition, the massive dense cores of our sample are in similar evolutionary stages, having not developed Ultra-compact HII regions yet (see Palau et al. 2014 for a more detailed discussion), and the Jeans mass depends more strongly on temperature than on density. For these reasons, we consider that the density structure of the massive dense cores in our sample is a reasonable approach to the density structure at the time of fragmentation.

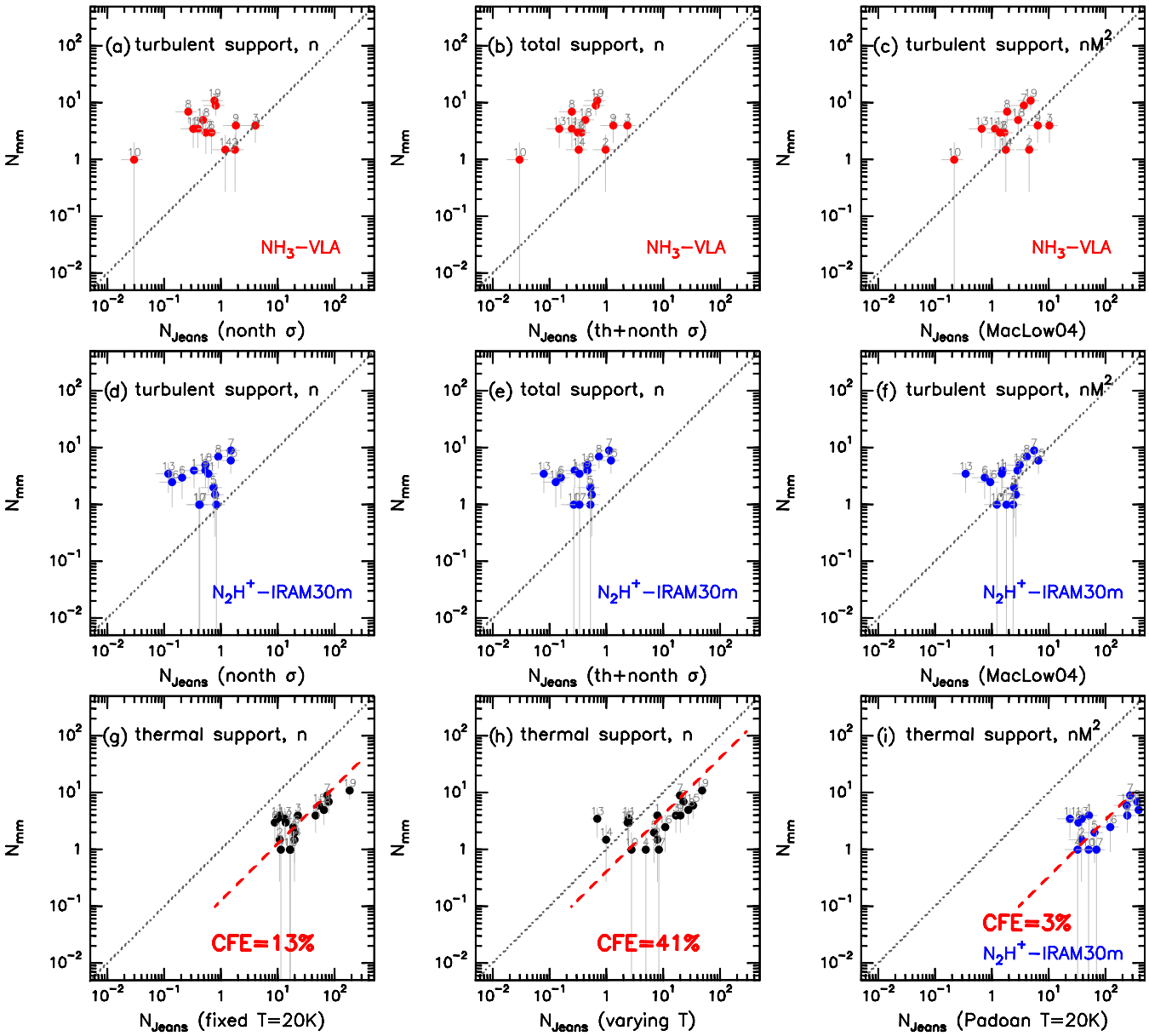

Figure 2. 'Fragmentation level' ($N_{\rm mm}$) versus Jeans number. Top panels: Jeans number calculated using the velocity dispersions estimated from NH_3, as explained in Section 3.2. Middle panels: idem but using the velocity dispersions estimated from N_2H^+ (Section 3.2). Bottom panels: Jeans number calculated considering only thermal support, calculated either using a fixed temperature of 20 K for all the cores (panels 'g' and 'i'), or the temperature inferred from the core modelling presented in Palau et al. (2014; panel 'h'; see Section 3.3). In all panels, the Jeans number is calculated using the average density inside a region of 0.1 pc of diameter (as explained in the table notes of Table 1; see also Palau et al. 2014), except for panels on the right, where the average density has been multiplied by the square of the Mach number (following Mac Low & Klessen 2004). In all panels, the dotted black line represents the one-to-one relation, for a core formation efficiency (CFE) of unity. For 'g', 'h' and 'i' panels, the red dashed line corresponds to the fit with slope =1 used to infer the indicated CFE (3–41 per cent).

Finally, we calculated the Jeans mass considering that turbulence is only producing regions of higher density, but not providing support against gravity (with the latter being only thermal, e.g. Padoan & Nordlund 2002):

$$\left[\frac{M_{\rm Jeans}^{\rm conv.flows-th}}{\rm M_\odot}\right] = 0.6285 \left[\frac{T}{10\,\rm K}\right]^{3/2} \left[\frac{n_{\rm H_2}\,\mathcal{M}^2}{10^5\,\rm cm^{-3}}\right]^{-1/2}. \quad (8)$$

We studied this case using Mach numbers calculated from NH_3 and N_2H^+ data (Table 1), and the results are listed in Table 2. The fit performed using NH_3 (to estimate the Mach number) has a correlation coefficient very similar to the coefficient obtained for pure thermal support at a fixed temperature of 20 K in Fig. 2(g), but the slope of the linear fit is significantly smaller (0.35 ± 0.11) and thus deviates more strongly from the one-to-one relation. As for the fit performed using N_2H^+ (to estimate the Mach number), the slope is more similar to the slope in Fig. 2(g). In Fig. 2(i), we show the case of N_2H^+ only for clarity. We also performed a linear fit forcing the slope to 1 to infer the CFE in this case, which is around 3 per cent for both NH_3 and N_2H^+ (see Table 2 and Fig. 2i). The CFE is very low because the densities in this case are higher (by

Table 2. Linear fits to the N_{mm} versus N_{Jeans} relations of Fig. 2, which correspond to different cases of core support.

Support[a]	Equation[a]	Panels Fig. 2[a]	Correlation coefficient[b]	Slope[b]	CFE[c] (per cent)	χ^{2c}
Turbulent (NH_3)	(2)	a, d	0.24	0.14 ± 0.18	>100 per cent	–
Turbulent (N_2H^+)	(2)	a, d	0.23	0.22 ± 0.25	>100 per cent	–
Turbulent $n\mathcal{M}^2$ (NH_3)	(5)	c, f	0.50	0.34 ± 0.18	$\gtrsim$100 per cent	–
Turbulent $n\mathcal{M}^2$ (N_2H^+)	(5)	c, f	0.36	0.33 ± 0.24	$\gtrsim$100 per cent	–
Thermal $T = 20$K	(6)	g	0.72	0.60 ± 0.14	13 per cent	1.27
Thermal varying T	(6)	h	0.57	0.34 ± 0.12	41 per cent	3.34
Thermal $T = 20$K $n\mathcal{M}^2$ (NH_3)	(8)	–	0.69	0.35 ± 0.11	3.7 per cent	2.37
Thermal $T = 20$K $n\mathcal{M}^2$ (N_2H^+)	(8)	i	0.64	0.47 ± 0.15	3.3 per cent	1.49

Notes. [a]Fits are performed for the relations of the panels (of Fig. 2) indicated in column (3), which correspond to N_{Jeans} estimated using the equations given in column (2).
[b]Correlation coefficient and slope of a linear fit with two free parameters. The slope should be close to one if the form of support correctly described the observations.
[c]Core formation efficiency inferred forcing a linear fit with slope = 1, and the corresponding χ^2.

$\mathcal{M}^2$) and the Jeans mass decreases resulting in a very high number of expected fragments.

Overall, the best correlation between N_{mm} and N_{Jeans} is found for the case of pure thermal support adopting a temperature of ∼20 K for all the cores and with no modification of the density by the Mach number (Fig. 2g). In addition, also for this case the slope in the N_{mm} versus N_{Jeans} relation is closest to 1 (see Table 2).

3.4 Fragment masses

We have estimated the masses of the fragments identified in each massive dense core by assuming the temperature at the distance of the fragment (from the core centre[6]) as provided by our modelled envelopes. We used the dust opacity law of Ossenkopf & Henning (1994; icy mantles for densities $\sim 10^6$ cm^{-3}). The results are shown in Fig. 3. About 45 fragments (out of 75) present masses <1 $M_\odot$. Although these masses have been inferred from interferometric observations using extended configurations, and thus part of the flux must have been filtered out by the interferometer, we estimate that the missed flux is probably not larger than a factor of ∼2 (the reason for this is that any fragment detected by the interferometer at such extended configurations must be intrinsically compact). For example, for the case of I22198, Sánchez-Monge et al. (2010) report a flux density at 1.3 mm using the Submillimeter Array (SMA) in compact configuration of ∼500 mJy, while Palau et al. (2013) report a flux density at 1.3 mm using the PdBI in its most extended configuration of ∼270 mJy (adding MM2 and MM2S). Thus, as a first reasonable approach, one might conclude that most of the fragments in our sample must have masses of the order of 1–2 $M_\odot$, or below.

On the other hand, the Jeans masses calculated for each region considering only thermal support for a fixed temperature of 20 K (shown as a solid line in Fig. 3) range from 0.4 to 1 $M_\odot$, with an average value of 0.75 $M_\odot$. If we use our second approach for the temperature, i.e. use the average temperature estimated for each core inside a region of 0.1 pc of diameter (Table 1, without including cores 13 and 14, whose temperature is clearly affected by stellar feedback), we find Jeans masses in the range from 1 to 5 $M_\odot$, with an average Jeans mass for all the regions of 2.2 $M_\odot$ (shown as a dashed line in Fig. 3). Since this last case should yield an upper limit

[6] The core centre is taken as the peak of the millimetre/submillimetre emission observed with a single dish (see Palau et al. 2014 for further details).

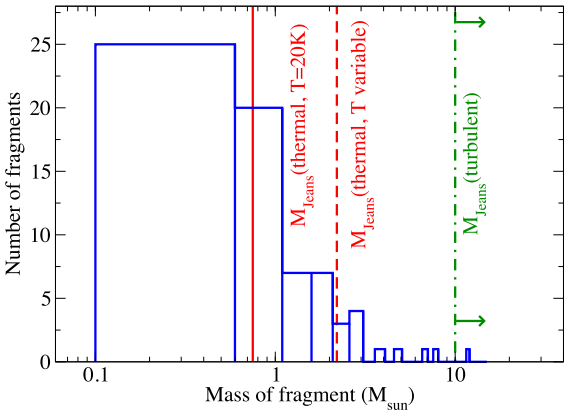

Figure 3. Histogram of fragments masses. The red solid line corresponds to the Jeans mass, averaged over all the sample, assuming thermal support at a fixed temperature of 20 K; the red dashed line corresponds to the Jeans mass, averaged over all the sample, assuming thermal support at the average temperature measured for each core inside a region of 0.1 pc of diameter (which should be an upper limit to the temperature at the time of fragmentation) and the green dot–dashed line corresponds to the Jeans mass, averaged over all the sample, assuming turbulent support as described in equation (5) (Mac Low & Klessen 2004). For the other prescriptions of turbulent support (Section 3.2), we obtain Jeans masses up to ∼80 $M_\odot$.

to the temperature at the time of fragmentation, the Jeans mass in this case is also an upper limit. For the case of average Jeans masses including the turbulence as a support term (equations 2, 4 and 5), these range from 10 (equation 5) up to ∼80 $M_\odot$ (equations 2 and 4). Therefore, we conclude that the typical masses of most of the fragments, around 1 $M_\odot$, are in good agreement with the Jeans mass considering pure thermal support only, with no need of additional forms of support.

4 DISCUSSION AND CONCLUSIONS

In the present work, we have investigated which process, turbulence or gravity, is controlling the fragmentation level of massive dense cores at a scale of ∼0.1 pc. We have used a sample of 19 massive cores, previously presented in Palau et al. (2013, 2014), to show that the fragmentation of these objects seems to be controlled mainly by thermal Jeans fragmentation. Specifically, we have shown that the fragmentation level, N_{mm} – measured as the number of compact fragments within a core – presents a significantly better correlation

with the core density than with its non-thermal velocity dispersion. Correspondingly, we have shown that $N_{\rm mm}$ correlates linearly with the number of fragments expected from simple thermal Jeans fragmentation, with a CFE, around 13 per cent, while, instead, assuming turbulence-dominated fragmentation, the majority of the cores should not fragment, contrary to what is observed. Finally, we have given hints that the masses of most of the fragments in our sample seem to be of the order of the Jeans mass calculated considering only pure thermal support.

4.1 Comparison to previous works

It is important to point out that our results are not inconsistent with those of Zhang et al. (2009), Pillai et al. (2011), Wang et al. (2011, 2014) and Lu et al. (2015). Those authors concluded that the fragments within massive cores of infrared-dark clouds have masses significantly larger than the thermal Jeans mass, and consistent with the turbulent-Jeans mass instead. However, in most of these clouds, this could be related to a sensitivity and spatial resolution issue due to the large distance of these infrared-dark clouds (ranging from 3.3 to 7.4 kpc). For example, in four (out of six) of those clouds, the mass sensitivity is >2 M$_\odot$ (above the Jeans mass) and the spatial resolution is >5000 au, while the massive dense cores studied here are all observed with mass sensitivities <1 M$_\odot$, and spatial resolutions $\sim$1000 au.

The most puzzling clouds are G28.34+0.06 P1 (Zhang et al. 2015), and the Snake (G11.11−0.12 P6, Wang et al. 2014). In these two clouds, observed down to subsolar mass sensitivities, there seems to be a lack of low-mass fragments, suggesting that the bulk of low-mass fragments have not formed yet at such earlier stages, or that the low-mass fragments form outside the core and follow the global collapse of the cloud. However, other recent multiwavelength studies focused on the stellar content of infrared-dark clouds show that most of the protostars formed in these clouds are of low-mass (<2 M$_\odot$; e.g. Samal et al. 2015), and thus this needs to be further investigated. Our study, carried out towards a sample of 19 regions more evolved than those in infrared-dark clouds, shows that most of the fragments detected in our sample are of low mass, and consistent with the thermal Jeans mass, indicating that at these stages the low-mass fragments do already exist. If the lack of low-mass fragments in infrared-dark clouds is confirmed in future observations, our data suggest that the duration of the stage when the low-mass fragments are formed is quite short. This is consistent with the extremely non-linear nature of the gravitational collapse (see e.g. fig. 1 (bottom left) of Toalá, Vázquez-Semadeni & Gómez 2012; fig. 1 of Zamora-Avilés & Vázquez-Semadeni 2014).

Finally, while it is possible that, in order to form the most massive fragments, additional compression mechanisms besides gravity may be necessary, the bulk of the fragmentation process in cores actively forming stars seems to be dominated by gravity rather than by turbulence. This is consistent with recent claims that the bulk of the non-thermal motions in clouds and cores may be dominated by infall rather than by random turbulence (e.g. Vázquez-Semadeni et al. 2008; Schneider et al. 2010; Ballesteros-Paredes et al. 2011a; Peretto et al. 2013; González-Samaniego et al. 2014; see also the review by Vázquez-Semadeni 2015).

4.2 Physical implications

Our results suggest that $N_{\rm mm}$ does not seem to depend significantly on the internal supersonic motions of the core, and are thus contrary to the widespread notion that support against gravity is necessary and that turbulence is the main physical process providing it and causing the fragmentation of molecular clouds. Since non-thermal supersonic motions are indeed observed in massive dense cores, but they do not seem to be random enough to act as a pressure against gravity, we propose that the observed 'turbulence' cannot be used to define a 'turbulent-Jeans' mass.

Although turbulence may very well play a crucial role in the formation of the seeds of what eventually will grow as cores, as demonstrated by the early evolution of molecular clouds in numerical simulations (e.g. Clark & Bonnell 2005; Vázquez-Semadeni et al. 2007; Heitsch & Hartmann 2008), one possible interpretation of our results is that the fragmentation process in star-forming regions is controlled mainly by gravitational contraction and the ensuing reduction in the thermal Jeans mass as the density increases during the collapse. Thus, a possibility is that the non-thermal motions are dominated by infall, produced by the gravitational contraction (e.g. Ballesteros-Paredes et al. 2011a). Indeed, analysis of the dense regions in simulations of driven, isothermal turbulence, indicate that the overdensities tend to have velocity fields with a net negative divergence (i.e. a convergence), rather than being completely random with zero or positive net divergence, as would be necessary for the bulk motions to exert a 'turbulent pressure' capable of opposing the self-gravity of the overdensities (Vázquez-Semadeni et al. 2008; González-Samaniego et al. 2014). Another possibility is that the non-thermal motions are strongly affected by stellar feedback, but in this case the effect on the clouds may be disruptive rather than supportive (Colín, Vázquez-Semadeni & Gómez 2013).

Our work supports the notion that non-thermal motions cannot be treated as capable of exerting a net turbulent pressure that can provide support against gravity and stabilize the cores, since we have found no evidence that the 'turbulent-Jeans mass' plays any significant role in the fragmentation of the cores. If this view is correct, then theoretical models based on the hypothesis of turbulent support (e.g. McKee & Tan 2003; Krumholz & McKee 2005) should be revised, as well as observational works that oversimplify the role of turbulence and estimate the Jeans mass by using an 'effective sound speed' corresponding to the non-thermal velocity dispersion. Clearly, a detailed comparison with simulations is needed to understand the origin of the non-thermal motions in massive dense cores and their role in the fragmentation process of molecular clouds. These simulations would help establish more clearly that gravity is indeed controlling fragmentation in massive dense cores at 0.1 pc scales, and even at scales of the entire molecular cloud once the clouds are well developed, as suggested by several authors (e.g. Clark & Bonnell 2005; Vázquez-Semadeni et al. 2007).

ACKNOWLEDGEMENTS

The authors are grateful to the anonymous referee for providing comments improving the clarity and quality of the paper. We wish to acknowledge useful and enjoyable discussions with Qizhou Zhang. AP is grateful to Jennifer Wiseman for sharing the NH_3 data, to Asunción Fuente, Tomás Alonso-Albi, Ke'nichi Tatematsu and Sylvain Bontemps for sharing the N_2H^+ data, and to Tim Jenness for sharing the James Clerk Maxwell Telescope data of IRAS 22198+6336 (Jenness et al. 1995). AP and LAZ acknowledge financial support from UNAM-DGAPA-PAPIIT IA102815 grant, and CONACyT, México. JBP thanks financial support from UNAM-PAPIIT grant number IN103012. ÁS.M. acknowledges support by the collaborative research project SFB 956, funded by the Deutsche Forschungsgemeinschaft (DFG). RE is partially supported by the Spanish MICINN grant AYA2011-30228-C03. GB is supported by

the Spanish MICINN grant AYA2011-30228-C03-01 (co-funded with FEDER funds). MF acknowledges the hospitality of the Aspen Center for Physics, which is supported in part by the US National Science Foundation under grant PHY-1066293. LG receives support from the Center of Excellence in Astrophysics and Associated Technologies (PFB-06), CONICYT (Chile) and CSIRO Astronomy and Space Science (Australia).

REFERENCES

Alonso-Albi T. et al., 2010, A&A, 518, A52
Audit E., Hennebelle P., 2005, A&A, 433, 1
Ballesteros-Paredes J., Hartmann L. W., Vázquez-Semadeni E., Heitsch F., Zamora-Avilés M. A., 2011a, MNRAS, 411, 65
Ballesteros-Paredes J., Vázquez-Semadeni E., Gazol A., Hartmann L. W., Heitsch F., Colín P., 2011b, MNRAS, 416, 1436
Bergin E. A., Hartmann L. W., Raymond J. C., Ballesteros-Paredes J., 2004, ApJ, 612, 921
Bonazzola S., Heyvaerts J., Falgarone E., Perault M., Puget J. L., 1987, A&A, 172, 293
Bontemps S., Motte F., Csengeri T., Schneider N., 2010, A&A, 524, A18
Busquet G., Estalella R., Zhang Q., Viti S., Palau A., Ho P. T. P., Sánchez-Monge Á., 2011, A&A, 525, A141
Chabrier G., Hennebelle P., Charlot S., 2014, ApJ, 796, 75
Chandrasekhar S., 1951, R. Soc. Lond. Proc. Ser. A, 210, 26
Clark P. C., Bonnell I. A., 2005, MNRAS, 361, 2
Colín P., Vázquez-Semadeni E., Gómez G. C., 2013, MNRAS, 435, 1701
Elmegreen B. G., 1993, ApJ, 419, L29
Federrath C., 2015, MNRAS, 450, 4035
Federrath C., Klessen R. S., 2013, ApJ, 763, 51
Fontani F., Caselli P., Crapsi A., Cesaroni R., Molinari S., Testi L., Brand J., 2006, A&A, 460, 709
Fontani F. et al., 2011, A&A, 529, L7
Fontani F., Busquet G., Palau A., Caselli P., Sánchez-Monge Á., Tan J. C., Audard M., 2015, A&A, 575, A87
Fuente A., Rizzo J. R., Caselli P., Bachiller R., Henkel C., 2005, A&A, 433, 535
Gerner T., Beuther H., Semenov D., Linz H., Vasyunina T., Bihr S., Shirley Y. L., Henning T., 2014, A&A, 563, A97
Gómez Y., Rodríguez L. F., Girart J. M., Garay G., Martí J., 2003, ApJ, 597, 414
González-Samaniego A., Vázquez-Semadeni E., González R. F., Kim J., 2014, MNRAS, 440, 2357
Guszejnov D., Hopkins P. F., 2015, MNRAS, 450, 4137
Hartmann L., Ballesteros-Paredes J., Bergin E. A., 2001, ApJ, 562, 852
Heitsch F., Hartmann L., 2008, ApJ, 689, 290
Heitsch F., Burkert A., Hartmann L. W., Slyz A. D., Devriendt J. E. G., 2005, ApJ, 633, L113
Hennebelle P., Chabrier G., 2008, ApJ, 684, 395
Hennebelle P., Chabrier G., 2011, ApJ, 743, L29
Hennebelle P., Pérault M., 1999, A&A, 351, 309
Heyer M., Krawczyk C., Duval J., Jackson J. M., 2009, ApJ, 699, 1092
Hopkins P. F., 2012, MNRAS, 423, 2037
Jenness T., Scott P. F., Padman R., 1995, MNRAS, 276, 1024
Jørgensen J. K., 2004, A&A, 424, 589
Kainulainen J., Beuther H., Henning T., Plume R., 2009, A&A, 508, L35
Kippenhahn R., Weigert A., Weiss A., 2012, in Astronomy and Astrophysics Library, Stellar Structure and Evolution. Springer-Verlag, Berlin, Heidelberg
Klessen R. S., 2000, ApJ, 535, 869
Klessen R. S., Heitsch F., Mac Low M.-M., 2000, ApJ, 535, 887
Koyama H., Inutsuka S.-i., 2002, ApJ, 564, L97
Kritsuk A. G., Norman M. L., Wagner R., 2011, ApJ, 727, L20
Krumholz M. R., McKee C. F., 2005, ApJ, 630, 250
Larson R. B., 1981, MNRAS, 194, 809
Léorat J., Passot T., Pouquet A., 1990, MNRAS, 243, 293
Louvet F. et al., 2014, A&A, 570, AA15
Lu X., Zhang Q., Wang K., Gu Q., 2015, ApJ, 805, 171L
Mac Low M.-M., Klessen R. S., 2004, RvMP, 76, 125
McKee C. F., Tan J. C., 2003, ApJ, 585, 850
Mangum J. G., Wootten A., Mundy L. G., 1992, ApJ, 388, 467
Ossenkopf V., Henning T., 1994, A&A, 291, 943
Padoan P., 1995, MNRAS, 277, 377
Padoan P., Nordlund Å., 2002, ApJ, 576, 870
Palau A., Sánchez-Monge Á, Busquet G., Estalella R., Zhang Q., Ho P. T. P., Beltrán M. T., Beuther H., 2010, A&A, 510, A5
Palau A. et al., 2013, ApJ, 762, 120
Palau A. et al., 2014, ApJ, 785, 42
Peretto N. et al., 2013, A&A, 555, A112
Pillai T., Kauffmann J., Wyrowski F., Hatchell J., Gibb A. G., Thompson M. A., 2011, A&A, 530, A118
Salim D. M., Federrath C., Kewley L. J., 2015, ApJ, 806, L36
Samal M. R. et al., 2015, A&A, 581, A5
Sánchez-Monge Á., Palau A., Estalella R., Kurtz S., Zhang Q., Di Francesco J., Shepherd D., 2010, ApJ, 721, L107
Sánchez-Monge Á. et al., 2013, MNRAS, 432, 3288
Sasao T., 1973, PASJ, 25, 1
Schneider N., Csengeri T., Bontemps S., Motte F., Simon R., Hennebelle P., Federrath C., Klessen R., 2010, A&A, 520, A49
Schneider N. et al., 2013, ApJ, 766, L17
Tatematsu K., Kandori R., Umemoto T., Sekimoto Y., 2008, PASJ, 60, 407
Tieftrunk A. R., Gaume R. A., Wilson T. L., 1998, A&A, 340, 232
Toalá J. A., Vázquez-Semadeni E., Gómez G. C., 2012, ApJ, 744, 190
Torrelles J. M., Ho P. T. P., Rodriguez L. F., Canto J., 1989, ApJ, 343, 222
Vázquez-Semadeni E., 2015, in Astrophysics and Space Science Library, Vol. 407, Magnetic Fields in Diffuse Media. Springer-Verlag, Berlin, Heidelberg, p. 401
Vázquez-Semadeni E., Gazol A., 1995, A&A, 303, 204
Vázquez-Semadeni E., Ballesteros-Paredes J., Klessen R. S., 2003, ApJ, 585, L131
Vázquez-Semadeni E., Ryu D., Passot T., González R. F., Gazol A., 2006, ApJ, 643, 245
Vázquez-Semadeni E., Gómez G. C., Jappsen A. K., Ballesteros-Paredes J., Gonzlez R. F., Klessen R. S., 2007, ApJ, 657, 870
Vázquez-Semadeni E., González R. F., Ballesteros-Paredes J., Gazol A., Kim J., 2008, MNRAS, 390, 769
Vázquez-Semadeni E., Gómez G. C., Jappsen A.-K., Ballesteros-Paredes J., Klessen R. S., 2009, ApJ, 707, 1023
Wang K., Zhang Q., Wu Y., Zhang H., 2011, ApJ, 735, 64
Wang K. et al., 2014, MNRAS, 439, 3275
Williams J. P., Blitz L., McKee C. F., 2000 in Mannings V., Boss A. P., Russell S. S., eds, Protostars & Planets IV. Tucson, AZ, Univ. Arizona Press, p. 97
Wiseman J. J., Ho P. T. P., 1998, ApJ, 502, 676
Zamora-Avilés M., Vázquez-Semadeni E., 2014, ApJ, 793, 84
Zhang Q., Wang Y., Pillai T., Rathborne J., 2009, ApJ, 696, 268
Zhang Q., Wang K., Lu X., Jimenez-Serra I., 2015, ApJ, 804, 141
Zhou S., Evans N. J., II, Mundy L. G., 1990, ApJ, 355, 159

APPENDIX A: FULL NAMES AND COORDINATES OF THE SAMPLE

In Table A1, we provide the full names or other names, coordinates and distances for the sources in our sample.

APPENDIX B: NH_3 AND N_2H^+ SPECTRA

In this appendix, we present the $NH_3(1,1)$ and $N_2H^+(1–0)$ spectra used in this work to estimate the non-thermal line widths for each massive dense core. The spectra, together with the hyperfine fits done using the CLASS program of GILDAS, are presented in Figs B1 and B2 and result from a compilation of data already published (see Section 2 for references) or reduced from the VLA archives.

APPENDIX C: NEW DENSITY AND TEMPERATURE DETERMINATION FOR IRAS 22198+6336

In Palau et al. (2014), the original images of IRAS 22198+6336 (I22198) published by Jenness et al. (1995) using the James Clerk Maxwell Telescope (JCMT) were not available, and the images were digitized. The images are now available and we have re-done the fit, with the additional difference (with respect to Palau et al. 2014) that the main beams assumed here are 7 and 14 arcsec at 450 and 850 μm, respectively, with no consideration of error beams. The results are presented in Fig. C1 and Table C1.

Table A1. Main properties of the sample of massive dense cores studied in this work.

Short name	Full name	Position[a] α(J2000)	Position[a] δ(J2000)	Distance (kpc)	L_{bol}[b] ($L_\odot$)	M_{obs}[c] ($M_\odot$)
1-IC1396N	IRAS 21391+5802	21:40:41.71	+58:16:12.8	0.75	290	78
2-I22198	IRAS 22198+6336	22:21:26.78	+63:51:37.6	0.76	340	115
3-N2071-1	NGC 2071	05:47:04.78	+00:21:43.1	0.42	440	80
4-N7129-2	NGC 7129-FIRS2	21:43:01.68	+66:03:23.6	1.25	460	81
5-CB3-mm	CB3-mm	00:28:42.70	+56:42:06.8	2.50	700	169
6-I22172N	IRAS 22172+ 5549-N	22:19:08.60	+56:05:02.0	2.40	830	119
7-OMC-1S	OMC-1S	05:35:14.00	−05:24:00.0	0.45	2000	158
8-A5142	AFGL 5142	05:30:48.02	+33:47:54.5	1.80	2200	356
9-I05358NE	IRAS 05358+3543-NE	05:39:13.07	+35:45:50.5	1.80	3100	1480
10-I20126	IRAS 20126+4104	20:14:26.04	+41:13:32.5	1.64	8900	68
11-I22134	IRAS 22134+5834	22:15:09.23	+58:49:08.9	2.60	11 800	222
12-HH80-81	IRAS 18162−2048	18:19:12.10	−20:47:30.0	1.70	21 900	333
13-W3IRS5	W3IRS5	02:25:40.77	+62:05:52.5	1.95	140 000	971
14-A2591	AFGL 2591	20:29:24.90	+40:11:19.5	3.00	190 000	784
15-Cyg-N53	Cygnus X-N53	20:39:03.10	+42:25:50.0	1.40	300	675
16-Cyg-N12	Cygnus X-N12	20:36:57.40	+42:11:27.5	1.40	320	622
17-Cyg-N63	Cygnus X-N63	20:40:05.20	+41:32:12.0	1.40	470	160
18-Cyg-N48	Cygnus X-N48	20:39:01.50	+42:22:04.0	1.40	4400	865
19-DR21-OH	DR21-OH	20:39:01.00	+42:22:46.0	1.40	10 000	526

Notes. [a]Approximate position of the centre of the field of view (corresponding to a region of ∼0.1 pc of diameter) where fragmentation was assessed in Palau et al. (2013, 2014).
[b]Bolometric luminosity as given in table 1 of Palau et al. (2014).
[c]M_{obs} is the mass computed analytically from the model of Palau et al. (2014), integrating until the radius where the density profile could be measured for each source. Note that for I22198 we present here an updated version of the model (see Appendix C).

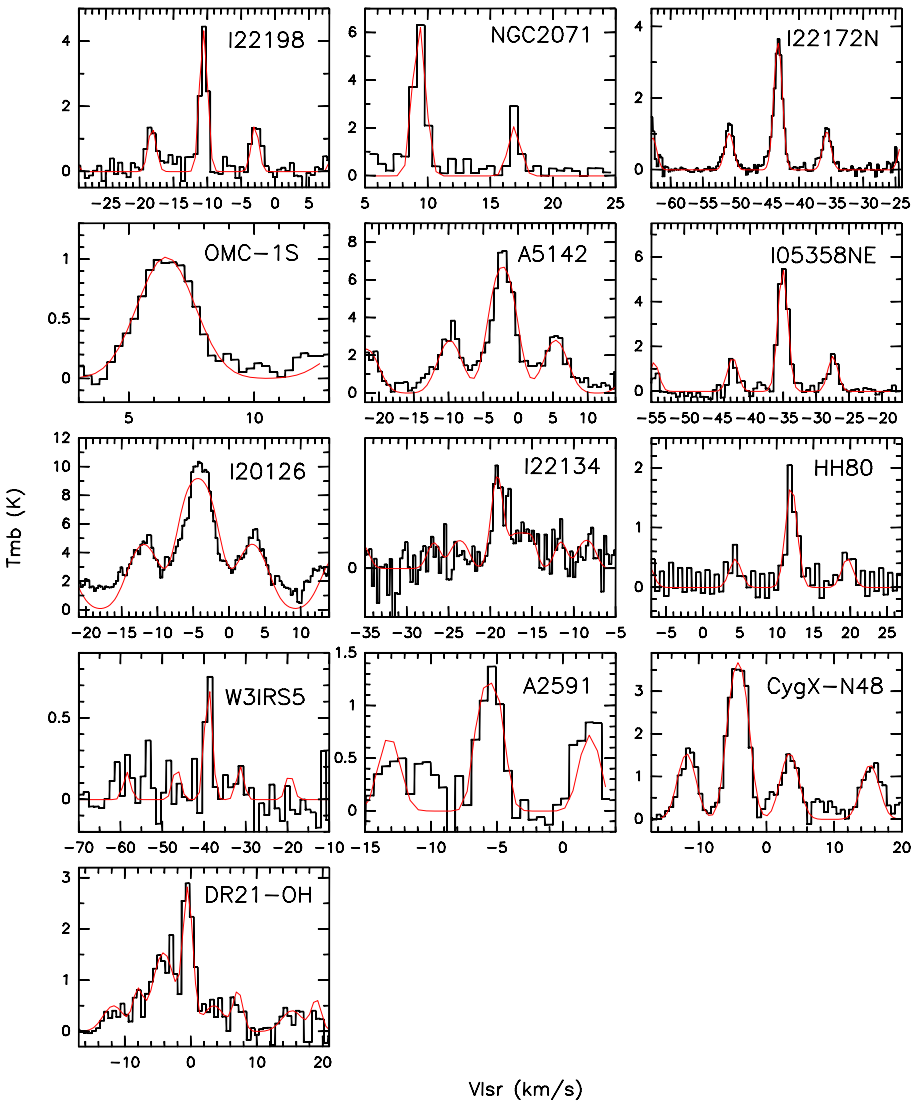

Figure B1. VLA $NH_3(1,1)$ spectra averaged over a region of ∼0.1 pc of diameter, where the fragmentation has been assessed. Red lines correspond to the CLASS fits to the hyperfine structure, from which the line width given in Table 1 has been inferred. For regions I22134 and DR21-OH, two velocity components have been used.

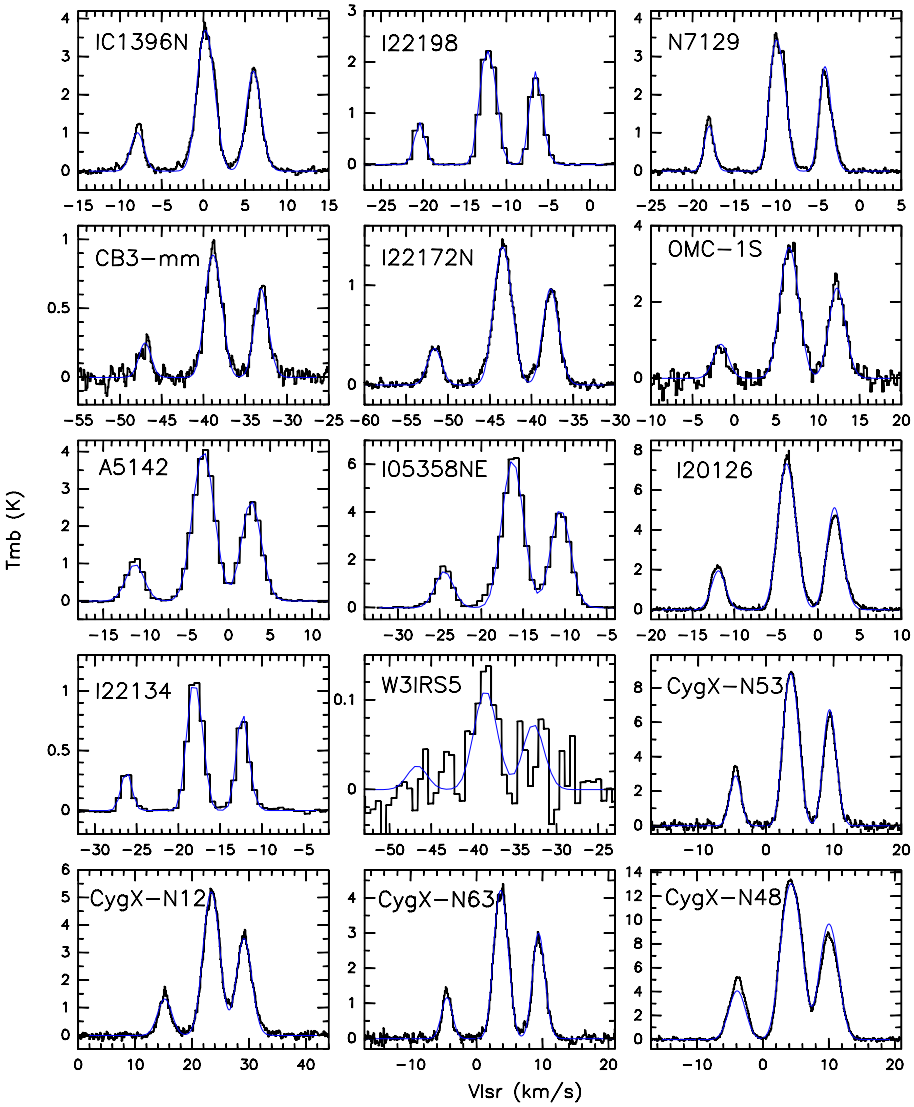

Figure B2. Single-dish N_2H^+(1–0) spectra averaged over a region of ∼0.1 pc of diameter, where the fragmentation has been assessed. Blue lines correspond to the CLASS fits to the hyperfine structure, from which the line width given in Table 1 has been inferred.

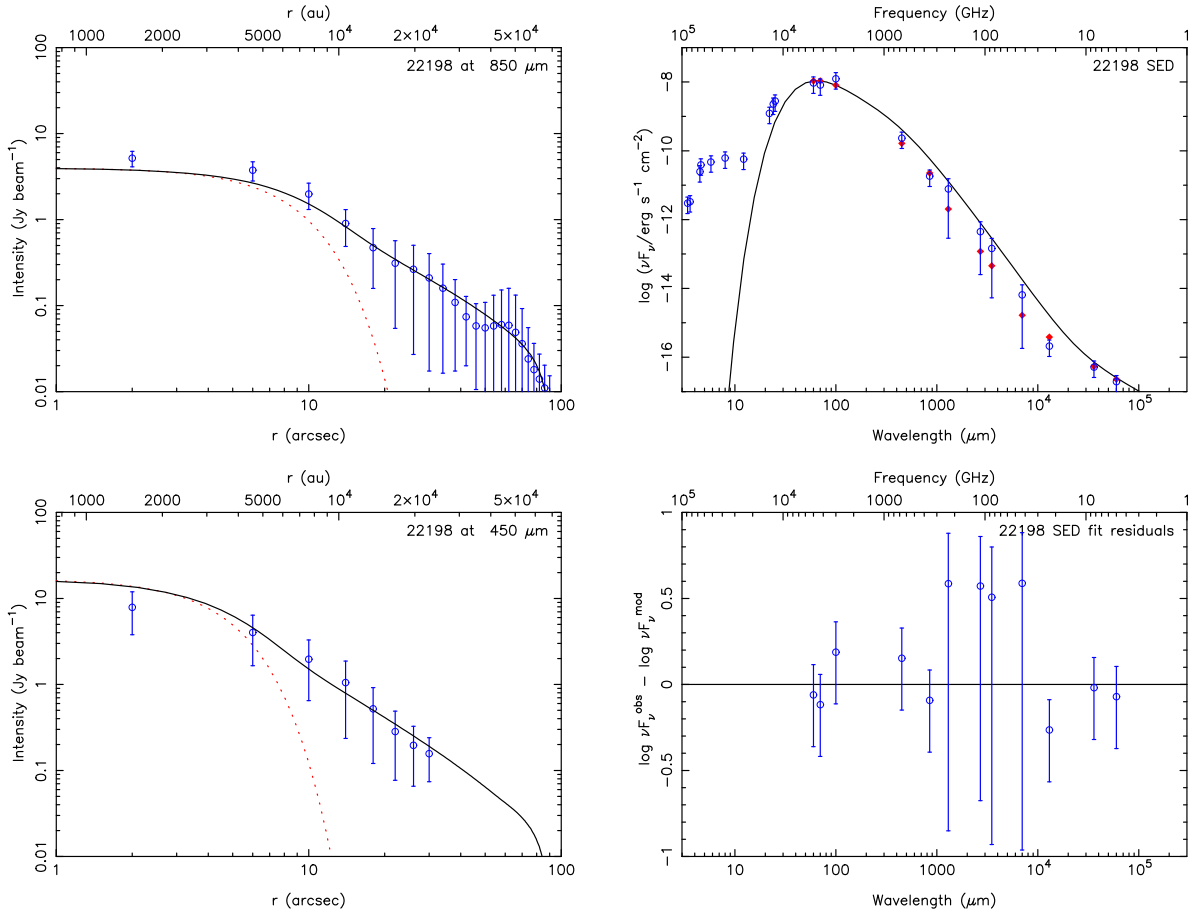

Figure C1. New fit (after Palau et al. 2014) to the radial intensity profiles and spectral energy distribution of IRAS 22198+6336 (I22198) after using original JCMT data of Jenness et al. (1995) work.

Table C1. Best-fit parameters to the radial intensity profiles and spectral energy distribution of IRAS 22198+6336 (I22198), and inferred properties (updated after Palau et al. 2014).

Source	β^a	$T_0{}^a$ (K)	$\rho_0{}^a$ ($\times 10^{-17}$ g cm^{-3})	p^a	$\chi_r{}^a$	q^b	$r_{10\,\mathrm{K}}{}^b$ (pc)	$r_{\mathrm{max}}{}^b$ (pc)	$M_{\mathrm{obs}}{}^b$ ($\mathrm{M}_\odot$)	$\Sigma_{0.1\,\mathrm{pc}}{}^b$ (g cm^{-2})	$n_{0.1\,\mathrm{pc}}{}^b$ ($\times 10^5$ cm^{-3})
I22198	1.16 ± 0.22	44 ± 4	3.4 ± 0.4	1.75 ± 0.03	0.580	0.39	0.22	0.31	115	0.29	3.6

Notes. [a]Free parameter fitted by the model: β is the dust emissivity index; T_0 and ρ_0 are the temperature and density at the reference radius, 1000 AU; p is the density power-law index; χ_r is the reduced χ as defined in equation 6 of Palau et al. (2014).
[b]Parameters inferred (not fitted) from the modelling. q is the temperature power-law index, and $r_{10\,\mathrm{K}}$ is the radius of the core where the temperature has dropped down to ∼10 K; r_{max} is the radius at the assumed 'ambient' density of 5000 cm^{-3}; M_{obs} is the mass computed analytically from the model integrating until the radius where the density profile could be measured for each source. $\Sigma_{0.1\,\mathrm{pc}}$ and $n_{0.1\,\mathrm{pc}}$ are the surface density and density inside a region of 0.1 pc of diameter.

This paper has been typeset from a TEX/LATEX file prepared by the author.